

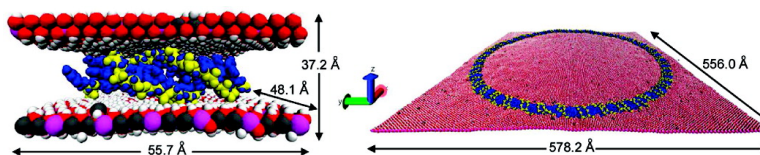
Article

## Computer Simulation Study of the Structural Stability and Materials Properties of DNA-Intercalated Layered Double Hydroxides

Mary-Ann Thyveetil, Peter V. Coveney, H. Chris Greenwell, and James L. Suter

*J. Am. Chem. Soc.*, **2008**, 130 (14), 4742-4756 • DOI: 10.1021/ja077679s

Downloaded from <http://pubs.acs.org> on February 8, 2009



### More About This Article

Additional resources and features associated with this article are available within the HTML version:

- Supporting Information
- Links to the 2 articles that cite this article, as of the time of this article download
- Access to high resolution figures
- Links to articles and content related to this article
- Copyright permission to reproduce figures and/or text from this article

[View the Full Text HTML](#)



**ACS Publications**  
 High quality. High impact.

## Computer Simulation Study of the Structural Stability and Materials Properties of DNA-Intercalated Layered Double Hydroxides

Mary-Ann Thyveetil, Peter V. Coveney,\* H. Chris Greenwell,<sup>†</sup> and James L. Suter

Centre for Computational Science, Department of Chemistry, University College London,  
20 Gordon Street, London WC1H 0AJ, United Kingdom

Received October 5, 2007; E-mail: p.v.coveney@ucl.ac.uk

**Abstract:** The intercalation of DNA into layered double hydroxides (LDHs) has various applications, including drug delivery for gene therapy and origins of life studies. The nanoscale dimensions of the interlayer region make the exact conformation of the intercalated DNA difficult to elucidate experimentally. We use molecular dynamics techniques, performed on high performance supercomputing grids, to carry out large-scale simulations of double stranded, linear and plasmid DNA up to 480 base pairs in length intercalated within a magnesium–aluminum LDH. Currently only limited experimental data have been reported for these systems. Our models are found to be in agreement with experimental observations, according to which hydration is a crucial factor in determining the structural stability of DNA. Phosphate backbone groups are found to align with aluminum lattice positions. At elevated temperatures and pressures, relevant to origins of life studies which maintain that the earliest life forms originated around deep ocean hydrothermal vents, the structural stability of LDH-intercalated DNA is substantially enhanced as compared to DNA in bulk water. We also discuss how the materials properties of the LDH are modified due to DNA intercalation.

### 1. Introduction

Layered double hydroxides (LDHs) are minerals which have a structure similar to that of brucite, whose formula is  $\text{Mg}(\text{OH})_2$ . LDHs form positively charged layers of metal hydroxides, with the general structural formula  $[\text{M}_{1-x}^{\text{II}}\text{M}_x^{\text{III}}(\text{OH})_2]^{x+}(\text{A}^{m-})_{x/m}\cdot y\text{H}_2\text{O}$ , where  $\text{M}^{\text{II}}$  are divalent metal cations,  $\text{M}^{\text{III}}$  are trivalent metal cations, and  $\text{A}^{m-}$  are interlayer anions which consist of a wide variety of inorganic and organic species.

Burgeoning interest surrounds the intercalation of nucleic acids into layered double hydroxides. Choy et al. have carried out extensive experiments showing that nucleotides including DNA can be intercalated into LDHs,<sup>1–5</sup> and that the metal hydroxide layers can protect DNA from catalytic and thermal degradation, making it possible for LDH–DNA intercalates to act as a molecular code system.<sup>4</sup> Choy has also discussed the possibility that DNA–LDH hybrid systems might act as non-viral vectors in which to transport DNA to cells for gene therapy,<sup>1–3,6</sup> the administered drug being carried in the interlayer

region of the LDH. The LDH reduces electrostatic repulsion between the negatively charged head groups of the lipid bilayer comprising the cell membrane and anionic DNA, increasing transfection efficiency.<sup>2</sup> An exhalation process might subsequently occur through ion exchange or degradation of the LDH in the slightly acidic ( $\text{pH} \approx 4\text{--}6$ ) cellular cytoplasm.

There are many different sizes and forms of DNA. For example, DNA can exist in single strand (ss) or double strand (ds) form. In addition to linear DNA, there also exist closed ds loops, called plasmids, which are commonly used in gene therapy.<sup>7</sup> Linear strands and plasmids can also exist as supercoiled structures, which often form when the DNA strand is under a twisting strain.<sup>8</sup> The experimental synthesis technique employed when making hybrid LDH–DNA systems has been shown to dictate the size of intercalated DNA.<sup>9</sup> The earliest experimental studies of LDH–DNA compounds showed that DNA of lengths between 200 and 300 base pairs (bps) could be intercalated from samples of free ds DNA molecules which were 100–5000 bps long, using an anion exchange technique.<sup>1–3</sup> However, LDHs have been found to intercalate larger linear and plasmid ds DNA between 100 and 8000 base pairs long using the coprecipitation method.<sup>9</sup> This method directly forms LDH around DNA, as opposed to anion exchange of DNA into pre-existing LDHs.<sup>10</sup>

<sup>†</sup> Present address: Department of Chemistry, Durham University, South Road, Durham DH1 3LE, UK.

(1) Choy, J.-H.; Kwak, S.-Y.; Park, J.-S.; Jeong, Y.-J.; Portier, J. *J. Am. Chem. Soc.* **1999**, *121*, 1399–1400.

(2) Choy, J.-H.; Kwak, S.-Y.; Jeong, Y.-J.; Park, J.-S. *Angew. Chem.* **2000**, *39*, 4041–4045.

(3) Choy, J.-H.; Kwak, S.-Y.; Park, J.-S.; Jeong, Y.-J. *J. Mater. Chem.* **2001**, *11*, 1671–1674.

(4) Choy, J.-H.; Oh, J.-M.; Park, M.; Sohn, K.-M.; Kim, J.-W. *Adv. Mater.* **2004**, *16*, 1181–1184.

(5) Choy, J.-H.; Son, Y.-H. *Bull. Kor. Soc.* **2004**, *25*, 122–126.

(6) Kwak, S.-Y.; Park, J.-S.; Jeong, Y.-J.; Choy, J.-H. *Solid State Ion* **2002**, *151*, 229–234.

(7) Pfeifer, A.; Verma, I. M. *Annu. Rev. Genomics Hum. Genet.* **2001**, *2*, 177–211.

(8) Calladine, C. R.; Drew, H. R. *Understanding DNA: The Molecule & How It Works*; Academic Press: New York, 1992.

(9) Desigaux, L.; Belkacem, M. B.; Richard, P.; Cellier, J.; Leone, P.; Cario, L.; Leroux, F.; Taviot-Gueho, C.; Pitard, B. *Nano Lett.* **2006**, *6*, 199–204.

(10) Miyata, S. *Clays Clay Miner.* **1983**, *31*, 305–311.

Increased structural stability of DNA is an important feature of LDH–DNA systems. Thermal stability up to 300 °C has been observed,<sup>4,9</sup> compared to typically less than 100 °C for DNA in bulk water. Increasing the temperature from ambient to 60 °C, a large contraction in interlayer spacing occurs in LDH–DNA systems,<sup>9</sup> along with an increase in the crystallinity of the interlayer. When probed further with thermogravimetric analysis, characteristic weight reductions indicative of loss of water (25–220 °C), dehydroxylation of the hydroxide layers (220–400 °C) and anion decomposition (above 450 °C) are observed. Furthermore, when the system is mixed with deoxyribonuclease, the intercalated DNA is found to resist degradation as the enzyme is unable to access the galleries.<sup>4</sup>

Other, more common minerals have also been found to interact with nucleic acids: mica,<sup>11</sup> montmorillonite<sup>12,13</sup> and kaolinite<sup>12,13</sup> have all been observed as surfaces on which DNA can be adsorbed. The interaction of RNA with montmorillonite is an example of a well documented clay–nucleic acid interaction. Ferris et al. have conducted experiments showing that montmorillonite can catalyze the oligomerization of suitably activated nucleotides to form strands of RNA.<sup>14,15</sup> This reaction is of importance to origins of life studies, which have yielded evidence that minerals may have played an important role in prebiotic synthesis.<sup>16–18</sup> Specifically, the RNA World hypothesis postulates that since RNA itself can act as a catalyst, in addition to carrying genetic information, the earliest forms of life were built upon RNA.<sup>19,20</sup>

Deep ocean hydrothermal vents have been suggested as possible sources for precursors of pre-biological molecules.<sup>21</sup> These include H<sub>2</sub>, N<sub>2</sub>, H<sub>2</sub>O, H<sub>2</sub>S, NH<sub>3</sub>, CH<sub>4</sub>, CO, CO<sub>2</sub>, HCN and P<sub>4</sub>O<sub>10</sub>. In such environments, it has been argued that minerals including LDHs could have further concentrated these primitive molecules, eventually leading to the formation of larger organic compounds.<sup>22,23</sup> Work by Pitsch et al.<sup>24</sup> and Krishnamurthy et al.<sup>25</sup> demonstrates that LDHs can catalyze the formation of sugar phosphates which form the backbone of nucleic acid polymers.

Although deep ocean hydrothermal vents have generated particular interest as a possible source of the first life forms,<sup>21</sup> there remains the question of how biopolymers such as RNA could have remained intact at the elevated temperatures and pressures around these vents. One possible explanation is that

clay-like particles may have acted as structures which supported and protected nucleic acids once formed. Experimentally, it has been shown that alkanes are formed when methanol reacts with smectites such as montmorillonite under conditions similar to those at hydrothermal seafloor vents.<sup>26</sup> Although LDHs are not as naturally common in present times, evidence suggests that during the earliest age of the Earth, called the Archean era, minerals such as green rust, [Fe<sup>II</sup>Fe<sup>III</sup>(OH)<sub>6</sub>]Cl·H<sub>2</sub>O, may have been much more common due to the lack of oxygen in the atmosphere.<sup>22</sup>

Research into the origins of life has rarely used simulation techniques to understand the possible chemical pathways to the formation of early biomolecules. The main purpose of the present paper is to use computer simulation to provide insight into the structure and stability of DNA while intercalated in layered materials, which is very difficult to obtain from experiment. Moreover, the flexibility of DNA–intercalated LDH is difficult if not impossible to obtain experimentally due to the small size of LDH platelets. Following simulation methods similar to those recently reported by us,<sup>27,28</sup> in this paper we use large-scale molecular dynamics to extract detailed information on the structure and dynamics of DNA intercalated within Mg<sub>2</sub>Al-LDH, as well as how the materials properties of Mg<sub>2</sub>-Al-LDH are modified when intercalated with DNA.

## 2. Methods

This section discusses the techniques we used to simulate selected LDH–DNA systems. We explain the choice of forcefield needed to describe the interaction between DNA and LDH. We use large-scale molecular dynamics to simulate systems containing up to one million atoms. A federation of three supercomputing grids was employed to perform the simulations as well as to visualize the data produced; since this is a somewhat novel computing infrastructure we also briefly describe pertinent aspects of it in this section.

**2.1. Model Construction.** The LDH used in this study was derived from an initial structure with chemical formula [Mg<sub>2</sub>Al(OH)<sub>6</sub>]Cl·2H<sub>2</sub>O. The primitive LDH structure was obtained by the refinement of powder X-ray diffraction (PXRD) data on hydrotalcite using Rietveld methods.<sup>29</sup> The crystallographic cell used to build our models was described using an *R*3*m* space group as this is the most commonly found in nature.<sup>30</sup>

The sizes and sequences of DNA molecules used in this study are given in Table 1. The smallest DNA molecule was created using the Amber Leap module and is a linear duplex dodecamer strand. The sequence of the DNA strand in system **I** was chosen as it has been well characterized in past molecular dynamics simulations<sup>31,32</sup> so a detailed understanding can be obtained of how its behavior changes while intercalated in LDH. The long DNA double strands in systems **II** and **III** were built using the Nucleic Acid Builder (<http://www.scripps.edu/mb/case/casegr-sh-3.2.html>). Systems **II** and **IV** consist of a linear ds DNA molecule, while system **III** is a closed circular ds loop. In the application of gene therapy, large strands of DNA including plasmids need to be intercalated into LDHs in order to transport genes.<sup>33</sup>

- (11) Pastré, D.; Piétrement, O.; Fusil, S.; Landousy, F.; Jeusset, J.; David, M.-O.; Hamon, L.; Le Cam, E.; Zozime, A. *Biophys. J.* **2003**, *85*, 2507–2518.
- (12) Franchi, M.; Ferris, J. P.; Gallori, E. *Origins Life Evol. Biosphere* **2003**, *33*, 1–16.
- (13) Pietramellara, G.; Franchi, M.; Gallori, E.; Nannipieri, P. *Biol. Fertil. Soils* **2001**, *33*, 402–409.
- (14) Ferris, J. P.; Ertem, G.; Agarwal, V. K. *Philos. Trans. R. Soc. London, Ser. B* **2006**, *361*, 1777–1786.
- (15) Ferris, J. P.; Ertem, G. *J. Am. Chem. Soc.* **1993**, *115*, 12270–12275.
- (16) Bernal, J. D. *Proc. Phys. Soc., London, Sect. B* **1949**, *62*, 597–618.
- (17) Cairns-Smith, A. G. *Genetic Takeover and the Mineral Origins of Life*; Cambridge University Press: Cambridge, 1982.
- (18) Arrhenius, G.; Sales, B.; Mojszsis, S.; Lee, T. *J. Theor. Biol.* **1997**, *187*, 503–522.
- (19) Gesteland, R.; Cech, T. R.; Atkins, J. F., Eds. *The RNA World*, 2nd ed.; Cold Spring Harbor Laboratory Press: Plainview, NY, 1999.
- (20) Wattis, J. A. D.; Coveney, P. V. *Int. J. Astrobiol.* **2005**, *4*, 63–73.
- (21) Wächtershäuser, G. *Philos. Trans. R. Soc. London, Ser. B* **2006**, *331*, 1787–1808.
- (22) Arrhenius, G. *Helv. Chim. Acta* **2003**, *86*, 1569–1586.
- (23) Greenwell, H.; Coveney, P. V. *Origins Life Evol. Biol.* **2006**, *36*(25, February), 13–37.
- (24) Pitsch, S.; Eschenmoser, A.; Gerdul, B.; Hui, S.; Arrhenius, G. *Origins Life Evol. Biol.* **1995**, *25*, 297–334.
- (25) Krishnamurthy, R.; Pitsch, S.; Arrhenius, G. *Origins Life Evol. Biol.* **1999**, *29*, 139–152.

- (26) Williams, L. B.; Canfield, B.; Voglesonger, K. M.; Holloway, J. R. *Geology* **2005**, *33*, 913–916.
- (27) Thyveetil, M.-A.; Coveney, P. V.; Suter, J. L.; Greenwell, H. C. *Chem. Mater.* **2007**, *19*, 5510–5523.
- (28) Suter, J. L.; Coveney, P. V.; Greenwell, H. C.; Thyveetil, M.-A. *J. Phys. Chem. C* **2007**, *111*, 8248–8259.
- (29) Bellotto, M.; Rebours, B.; Clause, O.; Lynch, J.; Bazin, D.; Elkaim, E. *J. Phys. Chem.* **1996**, *100*, 8527–8534.
- (30) de la Calle, C.; Pons, C.-H.; Roux, J.; Rives, V. *Clays Clay Miner.* **2003**, *51*, 121–132.
- (31) Jha, S.; Coveney, P. V.; Laughton, C. A. *J. Comput. Chem.* **2005**, *26*, 1617–1627.
- (32) Harris, S. A.; Gavathiotis, E.; Searle, M. S.; Orozco, M.; Laughton, C. A. *J. Am. Chem. Soc.* **2001**, *123*(50), 12658–12663.

**Table 1.** Simulation Cell Compositions and Dimensions for the Systems Containing Mg,Al-LDH Intercalated with DNA, Chloride Ions and Water

system	no. of atoms	no. of water molecules	no. of DNA base pairs (bps)	DNA sequence	starting supercell dimensions (Å <sup>3</sup> )
<b>I</b>	10,142	1406	12	d(5'-CTTTTGCAAAAAG-3')	49.0 × 56.5 × 54.0
<b>II</b>	344,959	23,328	108	d(5'-G <sub>27</sub> T <sub>27</sub> A <sub>27</sub> C <sub>27</sub> -3')	294.2 × 338.8 × 70.0
<b>III</b>	1,157,038	93,312	480	d([G <sub>121</sub> T <sub>119</sub> A <sub>119</sub> C <sub>121</sub> ]) <sub>2</sub>	588.3 × 677.7 × 70.0
<b>IV</b>	134,284	44,064	32	d(5'-G <sub>8</sub> T <sub>8</sub> A <sub>8</sub> C <sub>8</sub> -3')	140.5 × 112.0 × 85.9

<sup>a</sup> The DNA structures in models **I**, **II** and **IV** are all linear duplex strands, while model **III** consists of a closed circular loop of double-stranded DNA. System **IV** consists of linear double-stranded DNA in bulk water.

We chose to simulate a ring of DNA to emulate plasmid DNA used in gene therapy.<sup>7</sup> Experimentally, no record is available on the sequence of DNA intercalated into LDHs for chains longer than 100 base pairs, so we used arbitrary sequences for the long DNA chains in systems **II** and **III**. System **II**'s base pairs were sequentially arranged so that 27 of the same base pair were placed alongside each other, whereas system **III** had base pairs placed randomly. The DNA strand in system **IV** was simulated in bulk water in order to compare its behavior with intercalated DNA simulations. The sequence of base pairs in this DNA model was the same as that in system **II**, but the strand was a third of the length. To minimize interactions between DNA and its periodic images we imposed a minimum distance of 10 Å between DNA and the edge of the simulation box in system **I** and at least 20 Å in systems **II**, **III** and **IV**.

PXRD patterns of LDH–DNA systems are not as well defined as those of LDHs intercalated with simpler anionic species such as nitrate and chloride ions,<sup>2,9</sup> indicating a higher degree of disorder. Therefore, so as to simplify the model system and explore how the structure of DNA alters once intercalated in LDH, only one out of three LDH galleries was intercalated with DNA. The phosphate groups of all DNA strands were unprotonated with a unit negative charge. To conserve the overall charge neutrality of the system, chloride ions were also included in all LDH galleries. However, the same number of chloride ions as DNA phosphate groups was removed from the gallery containing the DNA molecule in order to keep the counterion charge distribution the same in each gallery. Figure 1 shows the initial structure of systems **I**, **II** and **III** before performing MD simulations. The models were parametrized with Amber's Leap module<sup>34</sup> and converted to LAMMPS input file format. The two DNA and LDH LAMMPS input files were aligned so that the DNA molecule was located within the central interlayer; the models were then combined to create the final structure. The combination of the two LAMMPS input files is possible because both the Amber forcefield<sup>35</sup> used to model DNA and the ClayFF forcefield<sup>36</sup> used to model LDH have the same functional form regarding bonding parameters. The functional forms of both forcefields are described in more detail in section 2.2.

The first part of our study aims to investigate the impact of hydration on system **I** by varying its water content. Models with varying degrees of hydration were created by changing the water content in the gallery containing DNA, while keeping the other two layers at two water molecules per unit formula Mg<sub>2</sub>Al(OH)<sub>6</sub>. The models also have a variety of different lateral dimensions. Previous studies of [Mg<sub>2</sub>Al(OH)<sub>6</sub>]·2H<sub>2</sub>O produced simulated hydration curves in general agreement with experimental results using the ClayFF forcefield intercalated with only chloride ions.<sup>27,37</sup> In addition, we have shown that finite size effects greatly affect the nature of clay simulations.<sup>27,28</sup> Thermal undulations

are emergent properties of simulations of LDHs<sup>27</sup> at length scales greater than the wavelength of the undulations, which is around 20 Å. Here too, therefore, we perform molecular dynamics simulations containing up to 1 million atoms in order to accurately model the interaction of long-chain DNA molecules with LDH. The models of LDH used in this study were created by replication of the primitive crystallographic cell, producing the model sizes detailed in Table 1. This study primarily aims to measure the in-plane elastic coefficients, so the simulation cell was replicated laterally along the basal plane, rather than increasing the thickness of the LDH. Further replication of the clay sheets in the z-dimension should not contribute significantly to the elastic constants; they are already well represented by virtue of the periodic boundary conditions imposed.

**2.2. Potential Parametrization.** We use classical molecular dynamics simulations to study the interaction of DNA with LDH. Interactions between minerals and organic molecules are difficult to describe with a single “standard” molecular mechanics forcefield. Most forcefields are parametrized for a specific organic or inorganic system. Previous simulations carried out on biomineral surfaces have coupled standard organic forcefields such as CHARMM<sup>38</sup> or CVFF<sup>39</sup> with inorganic forcefields using Schröder mixing rules in order to supply the missing Lennard-Jones parameters.<sup>40–42</sup> As the LAMMPS MD application we use to carry out our simulations does not admit Schröder mixing rules, Lorentz–Berthelot mixing rules were used to supply the missing Lennard-Jones parameters instead. Lorentz–Berthelot mixing rules estimate intermolecular potential parameters of the Lennard-Jones potential using an arithmetic average for the collision diameter and a geometric average for the well depth;<sup>43</sup> they work well in situations in which the dominant interactions are electrostatic, as is the case here (see Supporting Information for a breakdown of the potential energies and atomic charges).<sup>40</sup> A cutoff of 10 Å was imposed on the Lennard-Jones interactions. Coulombic interactions were computed using the Ewald summation and the particle–particle, particle–mesh method with a precision value of 0.001 and a grid order of 4.<sup>44</sup>

The Amber ff99 forcefield<sup>35</sup> provided parameters for the partial charges and bonded interactions within DNA molecules, while the ClayFF<sup>36</sup> forcefield furnished parameters for atoms within LDH. The Amber forcefield has been used extensively to simulate nucleic acids, and reproduces well the structure and dynamics of nucleic acid moieties, including Watson–Crick base pairing.<sup>45,46</sup> Similarly, ClayFF produces good agreement with experiment for layered double hydroxides in terms

(33) Radler, J. O.; Koltover, I.; Salditt, T.; Safinya, C. R. *Science* **1997**, *275*, 810–814.

(34) Case, D. A.; Cheatham, T. E., III; Darden, T.; Gohlke, H.; Luo, R.; Merz, K. M., Jr.; Onufriev, A.; Simmerling, C.; Wang, B.; Woods, R. J. *J. Comput. Chem.* **2005**, *26*, 1668–1688.

(35) Kollman, P. A.; Wang, J.; Cieplak, P. *J. Comput. Chem.* **2000**, *21*, 1049–1074.

(36) Cygan, R. T.; Liang, J.-J.; Kalinichev, A. G. *J. Phys. Chem. B* **2004**, *108*, 1255–1266.

(37) Wang, J.; Kalinichev, A. G.; Kirkpatrick, R. J.; Hou, X. *Chem. Mater.* **2001**, *13*, 145–150.

(38) MacKerell, A. D., Jr.; Brooks, B.; Brooks, L.; Nilsson, C. L., III; Roux, B.; Won, Y.; Karplus, M., Eds. *The Encyclopedia of Computational Chemistry*, 1st ed.; John Wiley & Sons: New York, 1998.

(39) Dauber-Osguthorpe, P.; Roberts, V. A.; Osguthorpe, D. J.; Wolff, J.; Genest, M.; Hagler, A. T. *Proteins: Struct., Funct., Genet.* **1988**, *4*, 31–47.

(40) Duffy, D. M.; Harding, J. H. *Langmuir* **2004**, *20*, 7630–7636.

(41) Cormack, A. N.; Lewis, R. J.; Goldstein, A. H. *J. Phys. Chem. B* **2004**, *108*, 20408–20418.

(42) Harding, J. H.; Duffy, D. M. *J. Mater. Chem.* **2006**, *16*, 1105–1112.

(43) Allen, M. P.; Tildesley, D. J. *Computer Simulation of Liquids*; Clarendon Press: New York, 1987.

(44) Hockney, R. W.; Eastwood, J. W. *Computer Simulation Using Particles*; Taylor & Francis, Inc.: Bristol, PA, 1988.

(45) Young, M. A.; Jayaram, B.; Beveridge, D. L. *J. Am. Chem. Soc.* **1997**, *119*, 59–69.

(46) Hobza, P.; Kabelac, M.; Sponer, J.; Vondrasek, J.; Mejzlík, P. *J. Comput. Chem.* **1997**, *18*, 1136–1150.

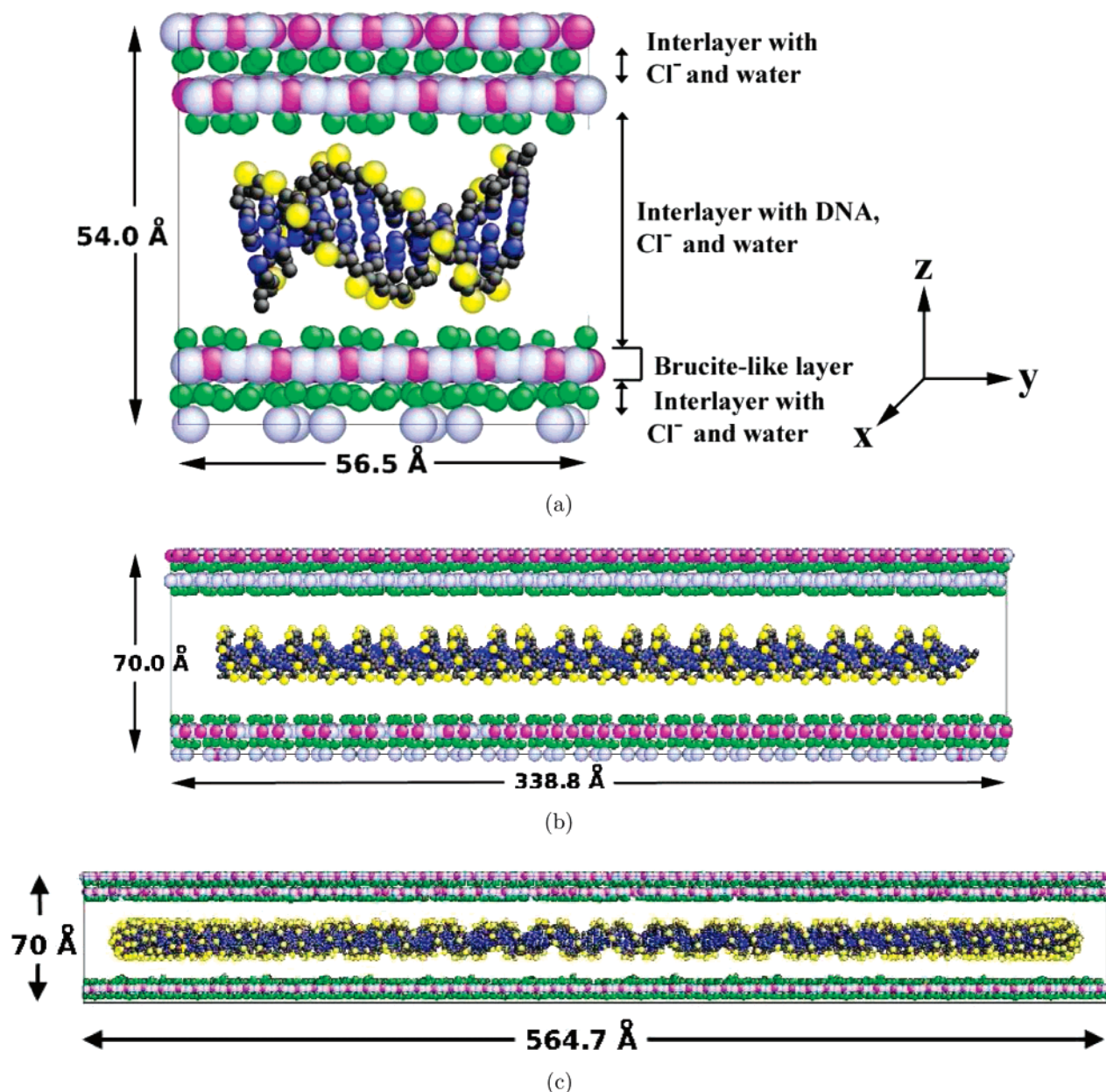


**Figure 1.** Starting structures of (a) system I; (b) system II; and (c) system III, in the  $yz$  plane. The major axis of the DNA strand in system I lies along the  $y$ -dimension, whereas in system II the major axes lies diagonally in the  $xy$  plane. Oxygen and hydrogen atoms have been removed in order to aid viewing. Magnesium, aluminum, chlorine, phosphorus, carbon and nitrogen atoms are represented as light-gray, pink, green, yellow, dark-gray and blue spheres respectively.

of lattice parameters, water diffusion coefficients and far-infrared spectra.<sup>37,47–49</sup> Both Amber and ClayFF use a harmonic potential for bond terms, while ClayFF is an ionic forcefield with no angle or dihedral terms, making the two forcefields relatively simple to combine. Water molecules are described using the flexible single-point charge (SPC) model.<sup>50</sup>

In addition to ambient conditions of 300 K and 1 atm, simulations were run at higher temperatures and pressures, as described in section 2.3. Under such conditions the validity of the potential parametrization is less secure. However, although detailed structural information may

be less reliable at higher temperatures and pressures, the simulations are expected to provide valuable insight into the behavior of LDH–DNA systems.

**2.3. Molecular Dynamics Techniques.** The large-scale atomistic/molecular massively parallel simulator (LAMMPS)<sup>51</sup> was used to simulate the LDH systems due to its highly scalable nature. The LDH models studied are identical to those in our previous study.<sup>27</sup> In addition, the simulations were performed at higher temperatures and pressures in order to gain insight into the structure of DNA under more extreme conditions while intercalated into LDHs. The simulations aim to reproduce the high temperatures and pressures around deep ocean hydrothermal vents.<sup>21</sup> Following energy minimization and thermalization,<sup>27</sup> 1-ns production simulations were performed. Those simulations run at 300 and 350 K were maintained at 1 atm pressure, the 400 K simulation was kept at 50 atm pressure, while the 450 and 500 K

(47) Kalinichev, A. G.; Kirkpatrick, R. J. *Chem. Mater.* **2002**, *14*, 3539–3549.

(48) Wang, J.; Kalinichev, A. G.; Amonette, J. E.; Kirkpatrick, R. J. *Am. Miner.* **2003**, *88*, 398–409.

(49) Wang, J.; Kalinichev, A. G.; Kirkpatrick, R. J. *Geochim. Cosmochim. Acta* **2006**, *70*, 562–582.

(50) Berendsen, H. J. C.; Postma, J. P. M.; von Gunsteren, W. F.; Hermans, J. *Intermolecular Forces*, 1st ed.; D. Reidel Publishing Co.: Dordrecht, The Netherlands, 1981.

(51) Plimpton, S. J. *Comput. Phys.* **1995**, *117*, 1–19.

simulations were held at 100 atm. System **IV**, a control simulation of DNA in bulk water, was similarly also studied under ambient conditions and at higher temperatures and pressures. The systems were judged to have reached equilibration before 500 ps by monitoring the potential energy and the cell parameters.

The interlayer structure was analyzed using one-dimensional atom density plots and radial distribution functions (RDF) (Thyveetil et al.<sup>27</sup>). Detailed structural information regarding the Watson–Crick hydrogen bonds in DNA was gleaned using the 3DNA software analysis tool<sup>52</sup> by least-squares comparison with crystal structures of model base pairs. In order to identify a Watson–Crick base pair, certain geometric criteria must be met: the distance between the origins of two bases must be less than 15 Å, the vertical separation must be less than 2.5 Å, the normal vectors of the base pairs must be rotated less than 65.0° with respect to each other and there must be at least one pair of nitrogen/oxygen base atoms that are within 4.05 Å of each other.<sup>53</sup>

A general measure of the structural stability is the root-mean-square deviation (rmsd) which quantifies the variation of the DNA from its initial structure. The rmsd is calculated using:

$$r_{\text{rmsd}}(\mathbf{r}, \mathbf{r}_0) = \sqrt{\frac{1}{N} \sum_{i=1}^N (\mathbf{r}_i - \mathbf{r}_{i,0})^2} \quad (1)$$

where  $\mathbf{r}$  is the current position of atom  $i$  and  $\mathbf{r}_{i,0}$  is its initial position. The initial position of DNA was taken from the starting structures, built using Amber. The summation is carried out over all  $N$  DNA atoms. The radius of gyration,  $r_G$ , quantifies how much stretching or compression the DNA molecules undergo:

$$r_G = \sqrt{\frac{1}{N} \sum_{i=1}^N (\mathbf{r}_i - \langle \mathbf{r} \rangle)^2} \quad (2)$$

where  $\langle \mathbf{r} \rangle$  is the mean position of all  $N$  DNA atoms;  $r_G$  can also be decomposed in each direction, where  $r_G^2 = r_{G,x}^2 + r_{G,y}^2 + r_{G,z}^2$ . The rmsd and RDF results are calculated by averaging the data from the production phase of the simulations. Error bars are obtained from the standard deviation of this data.

Principal component analysis (PCA) was used to describe the main changes in DNA morphology with time. Widely exploited to reduce the dimensionality of an MD trajectory, it identifies the dominant collective modes of motion of molecules.<sup>51,54–56</sup> In a Cartesian coordinate system, the covariance matrix can be defined as:

$$C = \langle (\mathbf{r} - \langle \mathbf{r} \rangle)(\mathbf{r} - \langle \mathbf{r} \rangle)^T \rangle \quad (3)$$

where  $\mathbf{r}$  represents the atomic positions of the DNA molecule in a  $3N$ -dimensional configuration space,  $\langle \mathbf{r} \rangle$  is the mean position of atoms over all snapshots and the superscript  $T$  denotes the transpose. In PCA, the eigenvectors and corresponding eigenvalues of  $C$  are found by diagonalization of the covariance matrix. The eigenvectors denote the orthogonal modes of motion, and the eigenvectors with the largest eigenvalues dominate the dynamics of the system.

**2.4. Determination of Materials Properties.** The elastic properties of clay sheets have been previously determined theoretically through uniaxial expansion and contraction of the simulation cell.<sup>27,28,57</sup> In this work we have used the same technique to obtain the components of the elastic modulus tensor,  $S_{ijkl}$ , as defined by the three-dimensional version of Hooke's Law:

$$\sigma_{ij} = \sum_{k=1}^3 \sum_{l=1}^3 S_{ijkl} \epsilon_{kl} \quad (4)$$

where  $\sigma_{ij}$  and  $\epsilon_{kl}$  are elements of the stress and strain tensors, respectively. The atomic coordinates are rescaled in order to fit the new geometry of the simulation box.

Our previous large-scale simulations of LDH sheets have shown that thermal undulations become apparent at larger system sizes but are not present for simulations comprising less than 50,000 atoms.<sup>27</sup> To illustrate the change in flexibility with system size, the height function of a single LDH sheet can be plotted.<sup>27,28</sup> The height function is found by partitioning the LDH sheet into a Cartesian grid in the  $xy$  plane, parallel to the LDH surface. The height function is defined as  $h(x,y) = z(x,y) - z_0$  where  $z_0$  is the mean  $z$  displacement of the LDH sheet and  $z(x,y)$  is the average  $z$  displacement at the center of each grid segment.<sup>27,28</sup>

**2.5. Grid Computing Infrastructure.** Very substantial computing resources were needed to perform the work reported here in a reasonable length of elapsed real time. To this end, grid computing facilities in Europe and the United States were utilized to carry out these studies. Simulations were performed on the following federated grid infrastructures: the UK's National Grid Service ([www.ngs.ac.uk](http://www.ngs.ac.uk)), including HPCx ([www.hpcx.ac.uk](http://www.hpcx.ac.uk)), the TeraGrid ([www.teragrid.org](http://www.teragrid.org)) and the EU Distributed European Infrastructure for Supercomputing Applications ([www.deisa.org](http://www.deisa.org)). System **III** was the largest model for which simulations were carried out, consisting of 1,157,038 atoms and requiring 50,000 CPU hours. Submission of jobs was facilitated by the Application Hosting Environment (AHE) (<http://www.omii.ac.uk/>).<sup>58</sup> AHE allows the submission of geographically distributed jobs through a single uniform interface which interoperates between Globus and Unicore grids and also retrieves output data automatically once a simulation has finished.

AtomEye-based visualization was used in order to quantitatively understand the evolution of the system. Parallel rendering of the trajectories was performed on six processors of an SGI Prism, further reducing time spent on visualization. Fast networks are required in order to transfer data from supercomputing resources for postprocessing and visualization. We used switched optical networking in order to transfer the large quantities of data generated in this study,  $\sim 250$  GB.<sup>59</sup> Specifically, we utilized the JANET lightpath research network (<http://www.ja.net/services/lightpath/>) which operates within the UK and connects to similar network infrastructures across Europe and the U.S.

### 3. Results and Discussion

#### 3.1. Impact of Hydration on Structural Stability of DNA.

The smallest DNA–LDH model, system **I**, was simulated in different hydration states to understand how the structural properties of the DNA change with varying water content. Our results show that, as in many previous studies carried out on the hydration properties of clays,<sup>60–62</sup> the amount of water in the interlayer region greatly impacts the structure of the system.

To our knowledge, there are no experimental hydration curves for Mg,Al-LDH/DNA systems although, at ambient temperatures, basal spacings reported from PXRD are between 21.1 and 23.9 Å.<sup>2,9</sup> This corresponds to ca. 9–11 water molecules per unit formula in system **I**. Other LDH–DNA systems, namely

(52) Lu, X.-J.; Olson, W. K. *Nucleic Acids Res.* **2003**, *31*, 5108–5121.  
 (53) Lu, X.-J.; Olson, W. K. <http://rutchem.rutgers.edu/xiangjun/3DNA/>, 2007.  
 (54) Hess, B. *Phys. Rev. E* **2000**, *62*, 8438–8448.  
 (55) de Groot, B. L.; Daura, X.; Mark, A. E.; Grubmuller, H. *J. Mol. Biol.* **2001**, *309*, 299–313.  
 (56) Amadei, A.; Linssen, A. B. M.; Berendsen, H. J. C. *Proteins* **1993**, *17*, 412–425.  
 (57) Manevitch, O. L.; Rutledge, G. C. *J. Phys. Chem. B* **2004**, *108*, 1428–1435.

(58) Coveney, P. V.; Saksena, R. S.; Zasada, S. J.; McKeown, M.; Pickles, S. *Comput. Phys. Commun.* **2007**, *176*, 406–418.  
 (59) Coveney, P. V.; Giupponi, G.; Jha, S.; Manos, S.; Suter, J. L.; Thyveetil, M.-A.; Zasada, S. J. Large Scale Computational Science on Federated International Grids: The Role of Switched Optical Networks. Preprint 2007.  
 (60) Newman, S. P.; Williams, S. J.; Coveney, P. V.; Jones, W. J. *Phys. Chem. B* **1998**, *102*, 6710–6719.  
 (61) Williams, S. J.; Coveney, P. V.; Jones, W. *Mol. Simul.* **1999**, *21*, 183.  
 (62) Greenwell, H. C.; Jones, W.; Coveney, P. V.; Stackhouse, S. *J. Mater. Chem.* **2006**, *16*, 708–723.

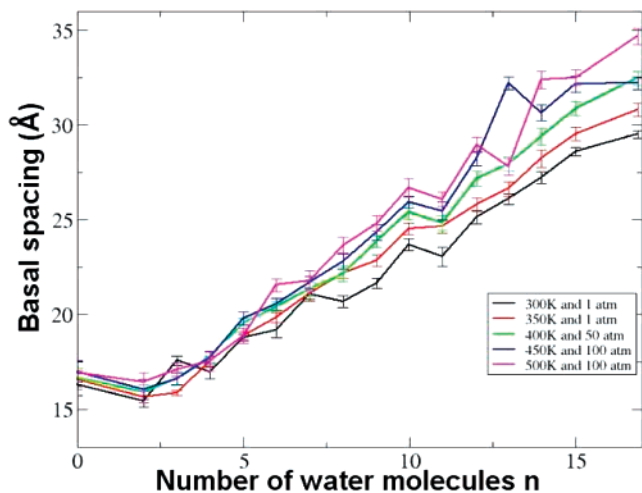


**Figure 2.** Simulated hydration curve for LDH–DNA system **I** at various temperatures and pressures. The values of the basal spacing were found by calculating the maximum distance between adjacent LDH layers. Steps in the hydration curve are due to the formation of water layers which develop on the LDH surface. Overall, a general increase in basal spacing is seen at greater temperatures and pressures;  $n$  corresponds to the number of water molecules per unit formula  $[\text{Mg}_2\text{Al}(\text{OH})_6] \cdot n\text{H}_2\text{O}$ . Error bars are derived by calculating the standard deviation of the maximum basal spacing throughout the simulations.

$\text{Mg}_2\text{Ga}\cdot\text{NO}_3\text{-DNA}$ ,<sup>9</sup> have been heated to temperatures as high as 400 °C at 1 atm pressure. At high temperatures there is a loss in water from  $\text{Mg}_2\text{Ga}\cdot\text{NO}_3\text{-DNA}$ , and the basal spacing shows significant reduction from 23.9 Å at room temperature to 18.6 Å at 60 °C.<sup>9</sup> Therefore, experimental and simulation results both indicate that hydration plays an important part in determining the basal spacing, and hence the structure of DNA when intercalated into LDHs.

Under ambient conditions the simulated swelling curve in Figure 2 shows steps, similar to the hydration of other clay systems,<sup>63,64</sup> including LDHs<sup>27,37</sup> with simple intercalated ionic species. Previous simulations have demonstrated that properties such as steps in hydration curves are an indication of hydrogen bonding between water and the clay surfaces. The organization of water molecules into well-defined layers induced by the polar surface means that additional water molecules can be adsorbed without a significant increase in basal spacing. Once these water layers become complete, a relatively large increase in the basal spacing arises as a second hydration layer starts to form.<sup>37</sup>

Our rmsd and  $r_G$  plots show that, within a dehydrated interlayer, the DNA is greatly distorted from its initial structure. Figure 3 shows the deformation which takes place with increasing water content. A more detailed study of the structure demonstrates that only with 10 water molecules per unit formula of  $\text{Mg}_2\text{Al-LDH}$  do all the Watson–Crick hydrogen bonds found in the initial structure remain intact, as shown in Figure 4. Figures 2 and 4 shows a deviant behavior at  $n = 13$ ; the fact that the standard deviation is in keeping with the other  $n$  values suggests that either a water molecule in this simulation may have been inserted in a local potential well resulting in slightly unusual configurations or that DNA is least deviated from its initial starting structure within hydration state  $n = 13$  at

temperatures above 450 K. With greater hydration, the water molecules may disrupt the DNA strand because of increased thermal motion. These results confirm the importance of water in supporting the DNA structure within the LDH sheets, an extreme example of the role of water influencing basal spacings in these materials.<sup>62</sup>

Figure 3a of system **I** in a dehydrated state shows that, viewed along the helical axis, the intercalated DNA has an almost rectangular cross section. This is due to the DNA phosphate backbone lying flat against the two LDH surfaces. All Watson–Crick hydrogen bonds are broken, and the backbone arranges itself so that most phosphate groups are in contact with the surface. With increasing hydration, the DNA adopts a more circular cross section when viewed along the helical axis, with fewer phosphates in contact with the surface.

To analyze the principal modes of motion within system **I** in different hydration states, PCA analysis was employed as discussed in section 2.3. In published MD simulations of DNA in bulk water, the dominant modes of motion are twisting of the helix around a central axis, as well as junction and wedge bending.<sup>65</sup> System **IV**, which contains DNA in bulk water, confirms this finding, but the intercalated DNA in systems **I–III** has different modes of motion since its backbone phosphate groups are pinned to the surface of the LDH, significantly restricting movement. At low hydration levels, the surface contact area between the DNA and the LDH sheets is relatively large, so the molecule remains virtually static. The main contribution to the dynamics at this hydration level is primarily seen at the ends of the DNA molecule. Figure 5 shows a superposition of all projections of atoms onto the first eigenvector, at different hydration levels. The superimposed projections show that, at higher levels of hydration, the backbone of the DNA exhibits more degrees of freedom—the main contribution to the dynamics arises from the motion of phosphate groups furthest away from the LDH surface. These phosphate groups oscillate toward and away from the central axis, tensioned by opposing forces of attraction toward the LDH surface and the hydrogen bonds between intra-DNA base pairs.

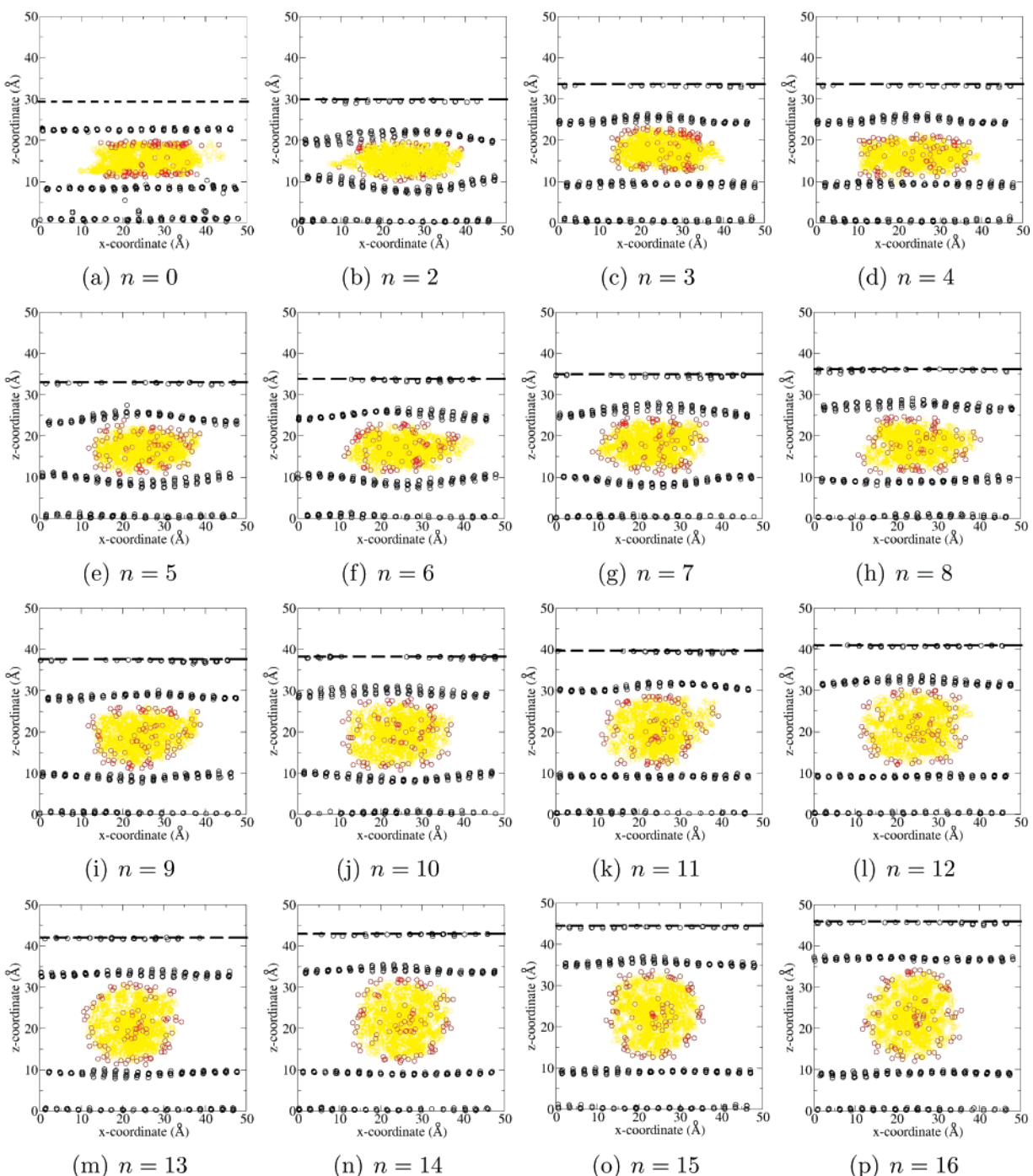
**3.2. Structural Stability of Intercalated DNA at Ambient Conditions.** At ambient temperatures and pressures, all models manifest structural stability of intercalated DNA. Although the DNA molecules in systems **I–III** are all compressed in the radial direction, visualization of the DNA trajectories shows that there is very little movement in the molecules while intercalated. Snapshots of systems **II** and **III** at the end of the simulations are shown in Figure 6. See also Supporting Information for animations of trajectories of systems **I–III**.

Figure 7 compares the XRD patterns of systems **I** and **II** with experimental studies of  $\text{Mg}_2\text{Al-NO}_3/\text{LDHs}$  intercalated with DNA.<sup>9</sup> Synthesized organo/LDH materials are often turbostratically disordered, causing adjacent clay sheets to be poorly ordered along the crystallographic  $c$  dimension. This manifests itself in broadened “saw-tooth”-shaped reflections, as seen in the pattern in Figure 7c. Also visible in Figure 7c are relatively sharp low-angle reflection peaks due to preferred ordering of anisotropic crystals during preparation of XRD samples. Organo/LDH systems are also highly sensitive to atmospheric humidity conditions, hydrating and dehydrating quite rapidly, making

(63) Boek, E. S.; Coveney, P. V.; Skipper, N. T. *J. Am. Chem. Soc.* **1995**, *117*, 12608–12617.

(64) Boek, E. S.; Coveney, P. V.; Skipper, N. T. *Langmuir* **1995**, *11*, 4629–4631.

(65) Sherer, E. C.; Harris, S. A.; Soliva, R.; Orozco, M.; Laughton, C. A. *J. Am. Chem. Soc.* **1999**, *121*, 5981–5991.



**Figure 3.** Cross section in the  $xz$  plane of system **I** in various hydration states at 300 K and 1 atm, taken from final snapshot of the simulation. The dashed black line corresponds to the length of the simulation cell along the  $z$ -axis. Black circles correspond to positions of aluminum ions in the LDH sheets. Periodic boundaries cause some aluminum ions to reside at the top of the simulation cell. The variable  $n$  refers to the number of water molecules per unit formula  $[\text{Mg}_2\text{Al}(\text{OH})_6] \cdot n\text{H}_2\text{O}$ . The atoms in phosphate groups are represented as red circles, while all other DNA atoms are yellow. When  $n > 9$  the structure of the DNA dodecamer duplex is preserved. In the anhydrous state ( $n = 0$ ), the DNA assumes a rectangular cross section, and phosphate groups align themselves with the surfaces of the LDH.

consistent, repeatable analysis difficult without resorting to a controlled relative humidity chamber. A further challenge to experimental analysis of LDHs based on X-ray diffraction is that, depending on the synthesis conditions, amorphous metal-oxide phases may be present which, though not discernible by XRD, may be identified when smaller-scale analysis such as energy dispersive spectroscopy is employed.<sup>66</sup>

Phosphate groups in the DNA backbone provide the dominant contribution to the electrostatic interaction between LDH sheets and DNA. The surface of each LDH sheet has discrete lattice points occupied by hydroxide groups and cations which represent key regions about which intercalated species generally organize themselves. For example, intercalated water molecules form hydrogen bonds with surface hydroxide groups.<sup>37</sup> More simple intercalated species, such as chloride ions, have been shown to adopt a loose arrangement around hydroxide groups.<sup>37</sup>

(66) Greenwell, H. C.; Marsden, C. C.; Jones, W. *Green Chem.* **2007**, *9*, 1299–1307.

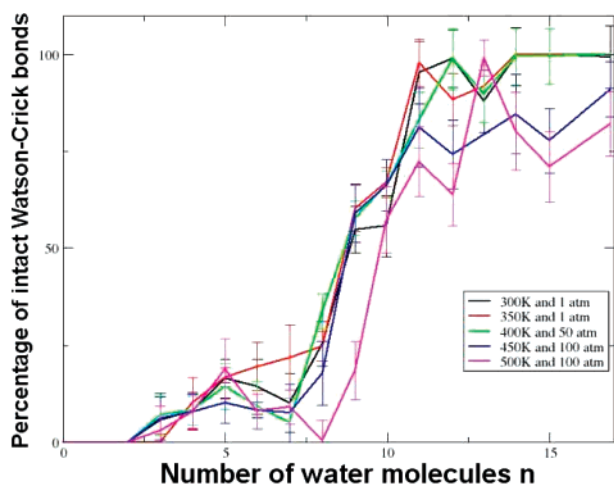


**Figure 4.** Average number and standard deviation of intact Watson–Crick base pairs for each simulation of system **I** performed at various temperatures and pressures. Water content in the interlayer containing DNA is varied as a function of  $[\text{Mg}_2\text{Al}(\text{OH})_6] \cdot n\text{H}_2\text{O}$ .

To allow the phosphate groups in DNA to organize themselves in the vicinity of positively charged regions of the clay, the DNA structure as a whole must be able to deform within the LDH.

Figure 8 displays the average radial distribution function of LDH atoms around phosphate groups, for all model sizes. Hydrogen atoms in LDH hydroxide groups and in water molecules make up the majority of atoms surrounding phosphate groups. Although the cations  $\text{Mg}^{2+}$  and  $\text{Al}^{3+}$  have similar RDFs, the closest peak is due to  $\text{Al}^{3+}$  ions which also has a greater intensity than that associated with  $\text{Mg}^{2+}$  ions, confirming that phosphate groups are attracted to regions on the surface of the LDH closer to  $\text{Al}^{3+}$  than  $\text{Mg}^{2+}$  sites.

Analysis of the average number of hydrogen bonds during the simulation for systems **II** and **III** shows that, even though the DNA is relatively restrained through the confinement imposed by the LDH gallery, the hydrogen bonding between base pairs is disrupted. System **I** has a higher percentage of intact Watson–Crick bonds at ambient temperatures compared to systems **II** and **III**. A possible explanation is that there are more DNA oligomers per LDH unit formula in system **I** than in the larger systems, hence increasing the number of interlayer atoms per unit formula, leading to larger basal spacings.

It has been suggested on the basis of circular dichroism experiments that DNA decreases in length in order to optimally align itself with  $\text{Al}^{3+}$  ions in the LDH sheets, resulting in a decrease in base pairs per turn from 10.4 to 10.2.<sup>67</sup> The RDF plot in Figure 8 for system **I** confirms that phosphate groups tend to align themselves closer to  $\text{Al}^{3+}$  than  $\text{Mg}^{2+}$  sites. We used the radius of gyration of DNA to determine whether it contracts or expands. After decomposing the radius of gyration of system **I** into its components along orthogonal axes, as shown in Figure 9, a general expansion of DNA can be seen in the  $x$ - and  $y$ -directions with increasing hydration. This DNA expansion, particularly along the  $y$ -axis (which is perpendicular to the helical axis), is in contrast to the foregoing interpretation of the circular dichroism experiments. However, the larger DNA molecules in systems **II** and **III** contract in the  $x$ - and

$y$ -directions, as shown in Figure 10; this may be due to the natural tendency of long-chain DNA to supercoil, which is quenched inside LDH. The Supporting Information contains snapshots that show evidence of DNA supercoiling at elevated temperatures. Reported MD simulations of smaller plasmids in bulk water exhibit supercoiling for simulations up to 80 ns.<sup>68</sup> Although our large-scale simulations have not been run for such an extended period, the rmsd values in Table 2 show that the plasmid is quite immobile while intercalated when compared to DNA in bulk water (system **IV**); extending the physical times of these simulations seems unlikely to show supercoiling of the DNA molecule under ambient conditions.

Principal mode analysis shows that the main motion within the larger intercalated DNA molecules is a collective movement which appears to correlate with the motion of the LDH sheets. Figure 11 shows the projection of the first eigenvector onto the backbone phosphate groups in systems **I–IV** and their associated probability density. See Supporting Information for data on the first three eigenvectors. The intercalated DNA molecules show a bimodal probability distribution in the first eigenvector, whereas DNA in bulk water shows a unimodal distribution. Generally, chains of DNA less than 20 base pairs long in bulk water have a well-defined equilibrium structure about which thermal motion takes place,<sup>65</sup> producing a unimodal Gaussian probability distribution in the projections of motion along each eigenvector. In addition, Figure 11 shows the subspace spanned by pairs of principal components for each system. It is clear that the trajectories in systems **II** and **III** occupy a narrow band which indicates that the eigenvectors are coupled. This behavior is diminished in systems **I** and **IV**, suggesting that the motions along each eigenvector are more independent of each other. The PCA results for systems **II** and **III** are similar to those seen in proteins such as lysozyme, which adopt multiple isomeric conformations.<sup>56,69</sup> Intuitively, it might be assumed that intercalated DNA would reach an equilibrium structure more quickly than DNA in bulk water due to confinement within the LDH sheets. As this is not the case, it suggests that there is a low-frequency force acting on intercalated DNA due to thermal motion of the LDH sheets. Previously, we have shown that simulation cells must be large enough to accommodate the thermal undulations of LDH sheets,<sup>27</sup> which are otherwise suppressed due to finite size effects.<sup>27</sup> As the coupled behavior of the principal modes becomes more pronounced with increasing system size, it suggests that the LDH sheets increasingly influence the motion of intercalated DNA for larger model sizes, most likely due to the thermal undulations which are more prevalent in systems **II** and **III** than system **I**.<sup>27</sup>

**3.3. Structural Stability of Intercalated DNA at Elevated Temperatures and Pressures.** The hydration curves of system **I** at various temperatures and pressures are shown in Figure 2. At higher than ambient temperatures the steps in the hydration curve are diminished, suggesting that the hydrogen bonds which support organized water layers are being disrupted by the increase in temperature. In general, the basal spacing increases with increasing temperature. This is most likely due to the greater thermal motion of water molecules in the interlayer region pushing the clay layers apart, as indicated by the atomic density profiles shown in Figure 12, which confirm that the

(67) Oh, J.-M.; Kwak, S.-Y.; Choy, J.-H. *J. Phys. Chem. Solids* **2006**, *67*, 1028–1031.

(68) Lankas, F.; Lavery, R.; Maddocks, J. H. *Structure* **2006**, *14*, 1527–34.

(69) Doruker, P.; Atilgan, A. R.; Bahar, I. *Proteins: Struct., Funct., Genet.* **2000**, *40*, 512–524.

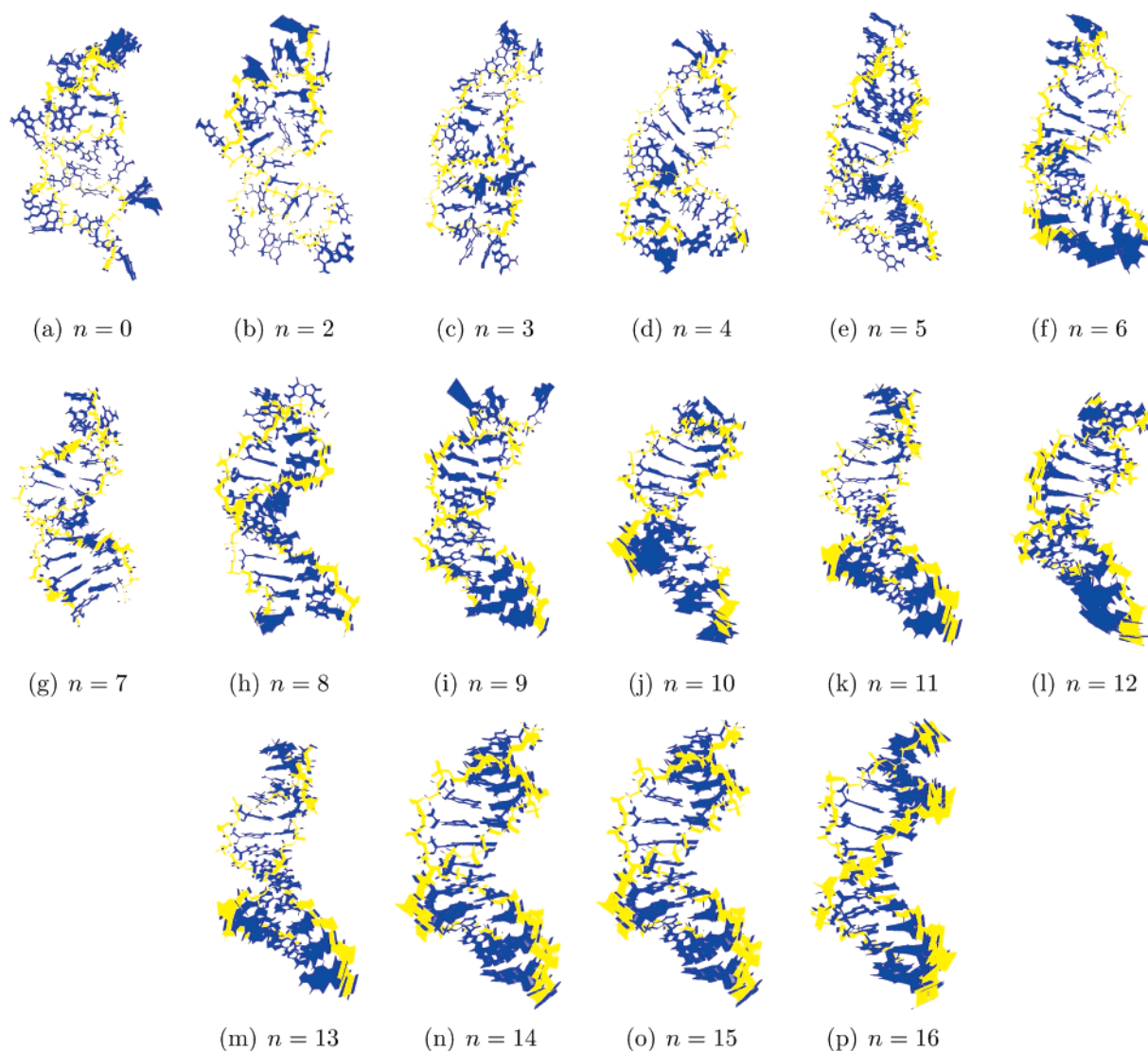


**Figure 5.** Superposition of configurations obtained by projecting the motion of all atoms onto the first eigenvector using principal component analysis of system **I**. The configurations are averaged over the last nanosecond of simulation for the studied hydration states, also shown in Figure 3. The variable  $n$  refers to the number of water molecules per unit formula  $[\text{Mg}_2\text{Al}(\text{OH})_6] \cdot n\text{H}_2\text{O}$ . The visualizations are viewed along the  $xy$  plane; the longitudinal axis of DNA lies parallel to the LDH sheets. Yellow represents the phosphate backbone, while blue includes the sugar groups and base pairs. At higher levels of hydration the phosphate groups furthest away from the LDH surface have more freedom to move.

positions of water molecules are less well defined at higher temperatures. The atomic density profiles of system **I** should not be broadened by thermal undulations as finite size effects restrict their formation in models of this size.<sup>27</sup>

The rmsd plots, computed with respect to the DNA strand's initial structure, of system **I** at different hydration states, temperatures and pressures are displayed in Figure 13. The plots enable us to infer that, with increasing hydration, the DNA strand becomes less distorted from its original structure. The rmsd plots also show that, at lower degrees of hydration, increasing the temperature and pressure does not produce a large difference in structure compared to more hydrated states. Since our PCA analysis shows that in dehydrated states very little movement is seen in the phosphate backbone, it can be deduced that, even at high temperatures and pressures, the movement of DNA is highly constrained.

As shown in Table 2, an interesting observation is that, as the temperature increases, the number of Watson–Crick base pairs increases in system **II**; hence, the intercalated DNA

becomes more stable, particularly when compared with DNA in bulk water (system **IV**). This is most likely due to the increase in basal spacing with temperature. This effect is not seen in the simulations of the smaller system **I**, where fewer Watson–Crick base pairs persist with increasing temperature. This may be due to the relative melting temperatures of the two DNA strands: smaller DNA molecules lose their helical structure at lower temperatures than longer DNA strands.<sup>70</sup>

**3.4. Corrugation of the LDH Sheets.** As noted above, most reported simulations of clay minerals, including smectites and LDHs, suffer from finite size effects which result in the suppression of thermal undulations in the clay sheets.<sup>27,28</sup> The largest wavelength found from the thermal undulations in  $[\text{Mg}_2\text{Al}(\text{OH})_6]\text{Cl} \cdot 2\text{H}_2\text{O}$  is 40 Å,<sup>27</sup> being larger than and unrelated to the initial models built. The simulations in the present study further demonstrate the flexibility of LDHs. The basal spacing between sheets enveloping DNA molecules is enlarged compared to that around intercalated chloride ions.

(70) SantaLucia, J., Jr. *Proc. Natl. Acad. Sci. U.S.A.* **1998**, *95*, 1460–1465.

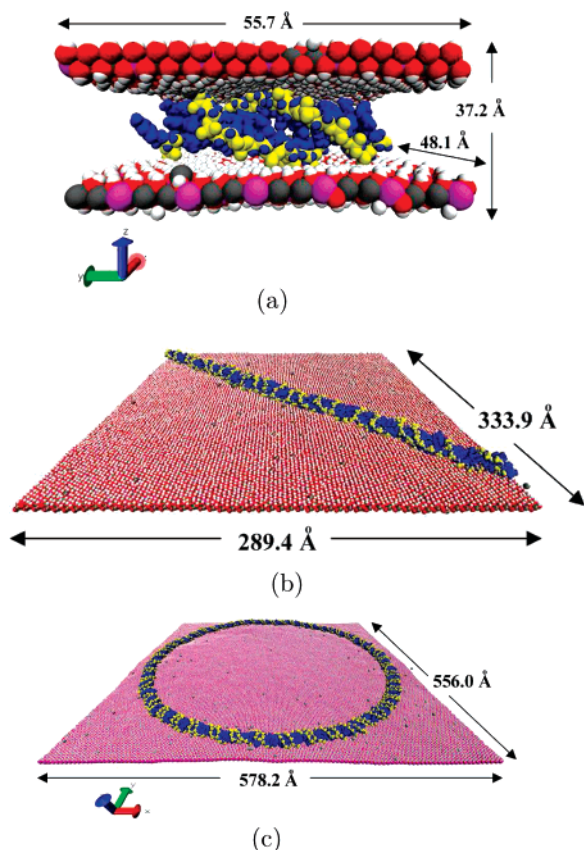
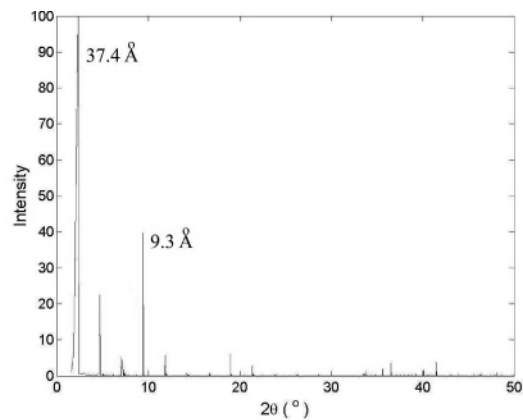


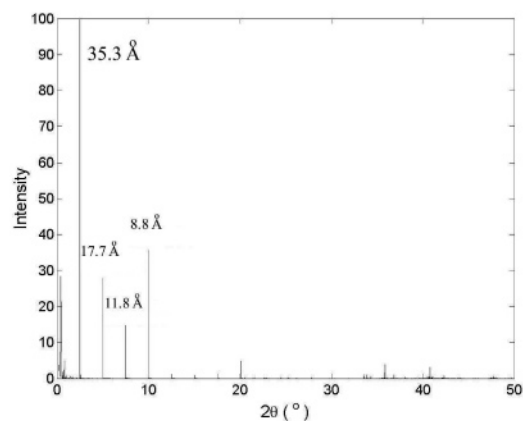
**Figure 6.** AtomEye visualizations of final snapshot for (a) system **I**; (b) system **II**; (c) system **III** under ambient conditions (300 K and 1 atm). Magnesium, aluminum, oxygen and hydrogen atoms in the LDH sheets are represented as gray, pink, red and white spheres, respectively. The DNA strand has been colored yellow to represent the phosphate backbone and blue for the sugar groups and base pairs. Water molecules have not been displayed and only one LDH sheet is visualized for systems **II** and **III**.

Although LDHs are more rigid than graphite,<sup>27,71</sup> the difference in size between DNA and chloride ions causes the sheets to distort around the large biopolymer. Figure 3 shows the position of  $\text{Al}^{3+}$  ions in the LDH sheets for different levels of hydration in system **I**. It is clear that lower levels of hydration cause a greater degree of bending within the LDH layers. The exceptional case (Figure 3a) is the anhydrous state which manifests no sheet distortions at all around the DNA. In this state all hydrogen bonds between DNA base pairs are completely ruptured, and the phosphate backbone of the DNA lies flat against the LDH surface; the LDH layers are not free to distort around the DNA molecule at least in part because chloride ions in neighboring interlayers keep adjacent LDH layers pinned close together through strong electrostatic bonds.

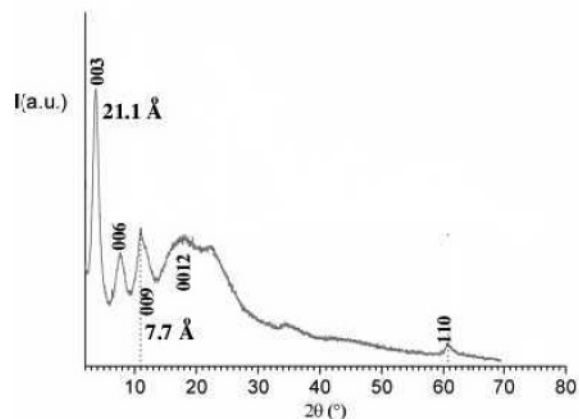
Systems **II** and **III** exhibit similar changes in basal spacing around regions of intercalated DNA. If the simulation cell is divided into a grid in the  $xy$ -plane, parallel to the LDH sheets, the basal spacing at each grid point can be found. By averaging this data over the production phase of the simulations, color map plots can be produced, as shown in Figure 14. A variation in basal spacing of 5 Å is seen within the interlayer occupied by DNA; in particular, the basal spacing is enlarged around the intercalated DNA. The minimum and maximum basal spacings within system **II** are 13.2 and 20.0 Å, respectively, whereas



(a)



(b)



(c)

**Figure 7.** Simulated powder X-ray diffraction spectrum for (a) system **I** and (b) system **II** compared with (c) experimental results reported by Desigaux et al.<sup>9</sup> Discrepancies exist between the simulated and experimental basal spacing which we attribute to the idealized nature of our simulations. Our simulations show peaks which are close to the limits of the experimentally measured diffraction peaks.

system **III** has respective values of 15.1 and 20.4 Å. Surrounding the enlarged interlayer region containing DNA is a depletion zone of approximately 20 Å, caused by the hydration of DNA.

Deformation in layered compounds is important for the mechanism of intercalation, since elastic properties determine whether a material shows intermediate stages upon intercalation.<sup>72</sup>

(71) Solin, S. A. *Annu. Rev. Mater. Sci.* **1997**, *27*, 89–115.

(72) Safran, S. A. *Phys. Rev. Lett.* **1980**, *44*, 937–940.

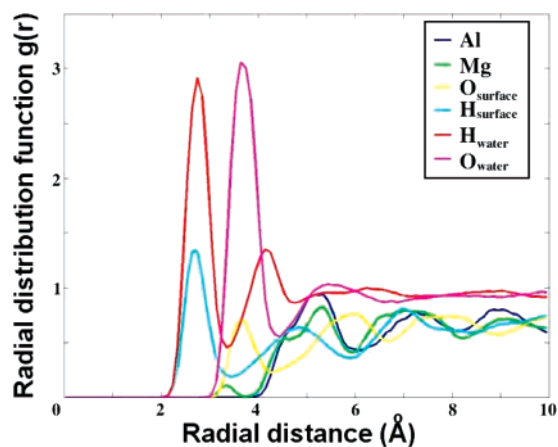


**Figure 8.** Average radial distribution functions for systems **I**, **II** and **III**, calculated with respect to phosphorus atoms in phosphate groups. The systems have 9 water molecules per unit formula  $[\text{Mg}_2\text{Al}(\text{OH})_6]$ , at a temperature of 300 K and pressure of 1 atm. Hydrogen atoms on the LDH surface and in water molecules have the largest density around phosphate groups.

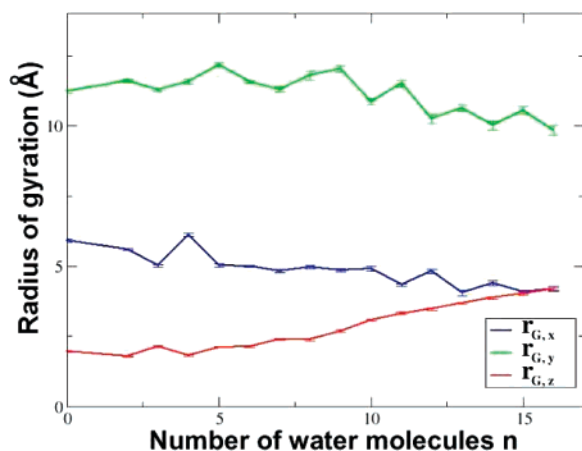


**Figure 9.** Components of the radius of gyration,  $r_G$ , for system **I** in different hydration states, projected along the  $x$ -,  $y$ - and  $z$ -directions at 300 K and 1 atm. The data show that the DNA dodecamer duplexes expand in the  $x$ - and  $y$ -dimensions with decreasing levels of hydration, while in the  $z$ -dimension the molecules become compressed.  $n$  corresponds to the number of water molecules per unit formula  $[\text{Mg}_2\text{Al}(\text{OH})_6] \cdot n\text{H}_2\text{O}$ .

Intermediate stages are formed when every  $n$ th layer is filled with intercalant, the remainder being vacant. Experimental studies of the process by means of which DNA intercalates in LDH systems have not thus far been reported, but based on our work we would expect that large molecules such as DNA may exhibit staging during the intercalation process. This is indirectly supported by experimental observations which show that those LDH systems exhibiting second-stage intermediates include bulky organic molecules, such as phosphonic acids of around 10 Å in length,<sup>73–75</sup> and large inorganic anions, such as perchlorate and iodide.<sup>76</sup>

**3.5. Elastic Properties of LDH–DNA Intercalates.** Stress–strain curves yield values for the Young’s moduli in each

- (73) Williams, G. R.; Norquist, A. J.; O’Hare, D. *Chem. Mater.* **2004**, *16*, 975–981.  
 (74) Fogg, A. M.; Freij, A. J.; Parkinson, G. M. *Chem. Mater.* **2002**, *14*, 232–234.  
 (75) Pisson, J.; Taviot-Gueho, C.; Israeli, Y.; Leroux, F.; Munsch, P.; Itie, J.-P.; Briois, V.; Morel-Desrosiers, N.; Besse, J.-P. *J. Phys. Chem. B* **2003**, *107* (35), 9243–9248.  
 (76) Iyi, N.; Fujii, K.; Okamoto, K.; Sasaki, T. *Appl. Clay Sci.* **2007**, *35*, 218–227.

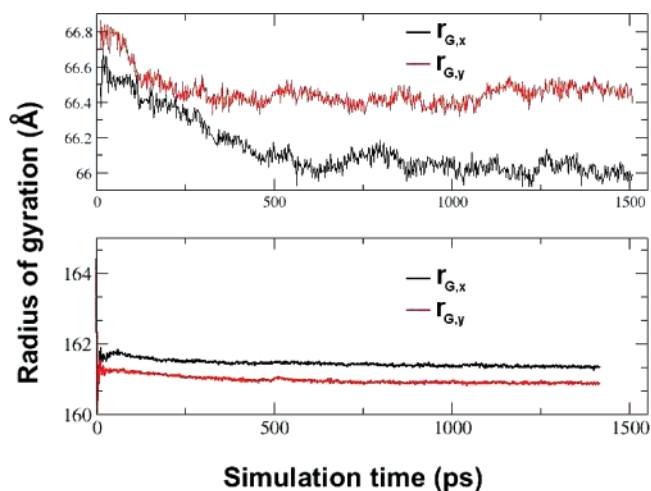


**Figure 10.** Radius of gyration,  $r_G$ , as a function of simulation time, decomposed in the  $x$ - and  $y$ -dimensions. The upper graph refers to the radius of gyration for system **II** and the lower one to system **III**. A contraction in the DNA molecules is seen, most likely due to their tendency to supercoil, but this behavior is largely quenched once intercalated within LDH sheets.

**Table 2.** Comparison of Systems **I**, **II** and **III** with 9 Water Molecules per LDH Unit Formula, in Terms of Hydrogen Bonds, Basal Spacing and rmsd of DNA Relative to Initial Structure

model	temperature (K)	pressure (atm)	number of Watson-Crick bonds	percentage of base-pairs	max. basal spacing (Å)	average rmsd (Å)
<b>I</b>	300	1	$7.2 \pm 0.7$	$60 \pm 6$	$21.7 \pm 0.3$	$2.2 \pm 0.1$
	350	1	$6.6 \pm 0.7$	$55 \pm 6$	$22.8 \pm 0.3$	$2.2 \pm 0.2$
	400	50	$6.9 \pm 0.4$	$58 \pm 2$	$23.9 \pm 0.3$	$2.2 \pm 0.2$
	450	100	$7.1 \pm 0.9$	$59 \pm 8$	$24.3 \pm 0.4$	$7.7 \pm 0.7$
	500	100	$2.2 \pm 0.7$	$18 \pm 6$	$24.8 \pm 0.4$	$8.9 \pm 0.9$
<b>II</b>	300	1	$20 \pm 1$	$19 \pm 1$	$20.0 \pm 0.1$	$6.8 \pm 0.3$
	350	1	$20 \pm 2$	$19 \pm 1$	$20.6 \pm 0.1$	$6.8 \pm 0.1$
	400	50	$23 \pm 3$	$21 \pm 3$	$21.9 \pm 0.1$	$6.7 \pm 0.1$
	450	100	$25 \pm 2$	$23 \pm 2$	$22.7 \pm 0.1$	$7.4 \pm 0.2$
	500	100	$30 \pm 2$	$28 \pm 2$	$23.7 \pm 0.1$	$8.0 \pm 0.1$
<b>III</b>	300	1	$70 \pm 3$	$15 \pm 4$	$20.4 \pm 0.1$	$8.1 \pm 0.1$
	500	100	$7 \pm 2$	$21.9 \pm 6$	–	$15 \pm 1$
<b>IV</b>	300	1	$25 \pm 1$	$78.1 \pm 3$	–	$6.5 \pm 0.8$
	350	1	$25 \pm 1$	$78.1 \pm 3$	–	$6.6 \pm 0.8$
	400	50	$12 \pm 2$	$37.5 \pm 6$	–	$10 \pm 2$
	450	100	$5 \pm 2$	$15.6 \pm 6$	–	$13 \pm 1$
	500	100	$7 \pm 2$	$21.9 \pm 6$	–	$15 \pm 1$

<sup>a</sup> The results are compared to system **IV** which is DNA in bulk water. Data is an accumulation of results obtained over the last 1 ns of simulation; the error bars are computed from the standard deviation of the data.

direction; these can be used to investigate how the elastic properties of the LDH change with the intercalation of DNA and with hydration. The Young’s modulus can be found for the whole system and separately for the LDH sheet alone. Table 3 summarizes the Young’s moduli in the  $x$ -,  $y$ - and  $z$ -directions for systems **I–III** with the same ratio of water molecules per unit formula, and compares these with results obtained for LDH–Cl.<sup>27</sup> The Young’s moduli for all LDH–DNA system sizes have similar values. The Young’s moduli for LDH sheets plus interlayer for systems **I–III** yield values of  $52 \pm 1$  GPa in the  $x$ -direction,  $52 \pm 1$  GPa in the  $y$ -direction, and  $22 \pm 2$  GPa in the  $z$ -direction. The results show that the LDH–DNA system is more flexible than LDH–Cl, whose elastic properties are given in Table 3.<sup>27</sup>

The elastic constants of system **I** in different hydration states were calculated to investigate whether hydration plays a role in the flexibility of the system. Figure 15a shows that the elastic constants for the LDH sheets plus interlayer display a general

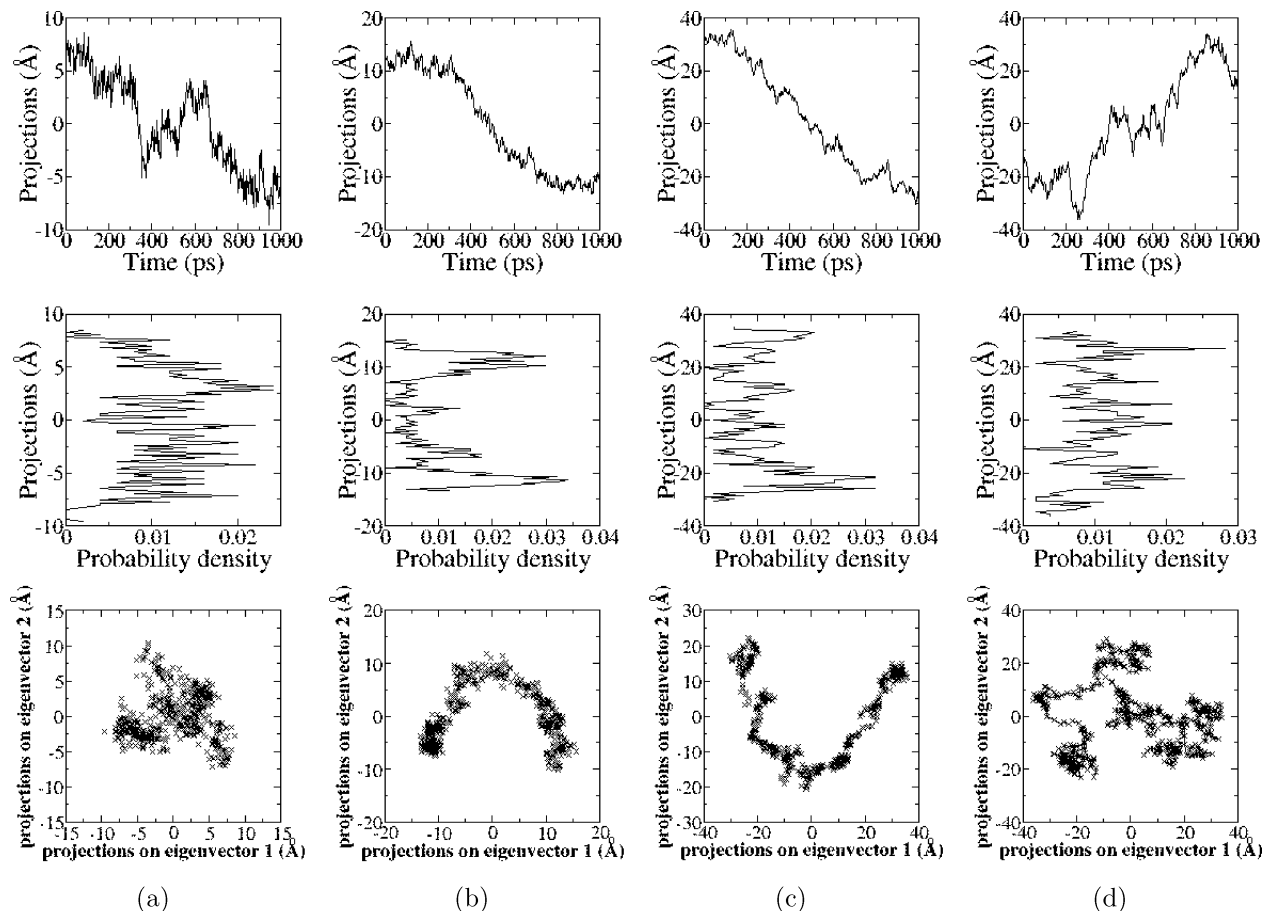


**Figure 11.** Principal component analysis of DNA intercalated within partially ion-exchanged  $[\text{Mg}_2\text{Al}(\text{OH})_6]\text{Cl}\cdot 9\text{H}_2\text{O}$ . Motions along the first eigenvector obtained from coordinates of the phosphate backbone and their planes of motion defined by the first two eigenvectors of (a) system I; (b) system II; (c) system III; and (d) system IV. A bimodal probability distribution is observed for intercalated DNA; as the motion of intercalated DNA is restricted the principal modes are heavily influenced by the thermal motion of the LDH sheets. Systems II and III show strong dependencies between the first two eigenvectors, suggesting that forces acting along these eigenvectors are coupled.

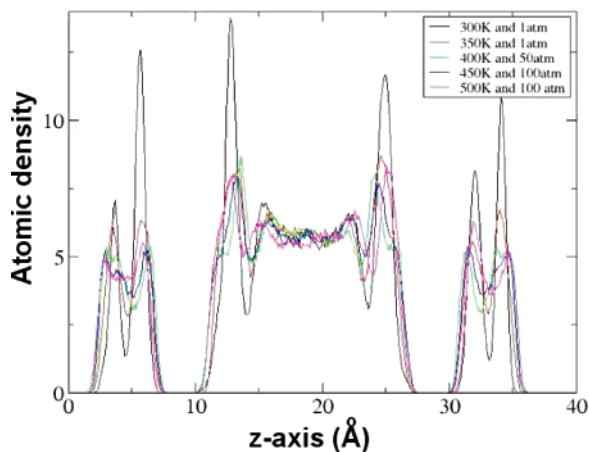


**Figure 12.** Atomic density profiles orthogonal to LDH sheets for oxygen atoms in water molecules of system I at different temperatures and pressures. The profiles are computed as averages over the production phase of each simulation. At ambient temperature and pressure, the distribution of water molecules is highly structured, as hydrogen bonds are formed between oxygen atoms in the water and surface hydroxide groups. With increasing temperature and pressure, the interlayer becomes less structured, hydrogen bonds between the water and LDH surface being increasingly ruptured.

reduction in rigidity with water content, due to the weakening of van der Waals and electrostatic forces between adjacent LDH sheets with increased hydration. This shows that the reduction in rigidity of LDH–DNA systems compared to that of LDH–

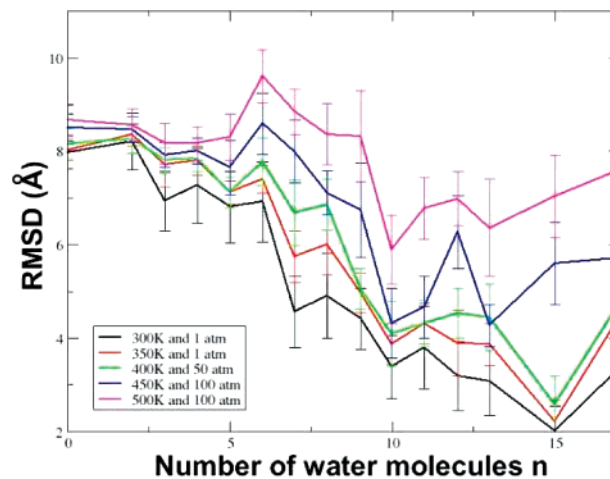


**Figure 13.** Root-mean-square deviation of DNA for system I at different temperatures and pressures, relative to the initial structure. At higher levels of hydration, the structure of DNA coincides with the starting structure, whereas increasing the temperature and pressure increases the distortion of the intercalated DNA duplex from the original structure.  $n$  refers to the number of water molecules per unit formula  $[\text{Mg}_2\text{Al}(\text{OH})_6]\cdot n\text{H}_2\text{O}$ .

Cl is most likely due to the increased water content within the central interlayer. The LDH–Cl model studied by Thyveetil et al.<sup>27</sup> had a water content of  $n = 2$  for unit formula  $[\text{Mg}_2\text{Al}(\text{OH})_6]\cdot n\text{H}_2\text{O}$ . For system I with the same number of water molecules in the interlayer containing DNA, the Young's moduli

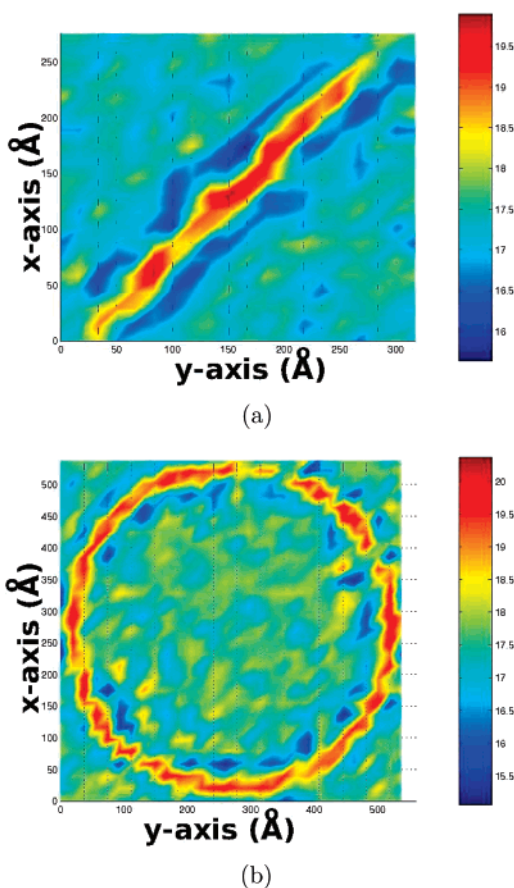


**Figure 14.** Color-scale plots showing the change in basal spacing of the LDH around intercalated DNA. The images were created by averaging the distance between adjacent layers throughout the simulation for (a) system **II** which has maximum and minimum basal spacings of 20.0 and 13.3 Å, respectively, (b) system **III** which has maximum and minimum basal spacings of 20.4 and 15.1 Å, respectively. Regions of the LDH sheets directly above or below DNA have the largest basal spacings. Regions with the largest basal spacings are colored red, while regions with the smallest basal spacings are colored blue.

**Table 3.** Young's Moduli in GPa for Systems **I**, **II** and **III**, Calculated from Stress–Strain Behavior of (i) the Whole System Containing the LDH–DNA and (ii) Only the LDH Sheet

system	(i) whole system			(ii) LDH sheet	
	$E_x$	$E_y$	$E_z$	$E_x$	$E_y$
<b>I</b>	$52 \pm 1$	$53 \pm 1$	$20 \pm 2$	$149 \pm 2$	$149 \pm 3$
<b>II</b>	$52.1 \pm 0.4$	$52.1 \pm 0.5$	$21.4 \pm 0.7$	$142.3 \pm 0.9$	$143.7 \pm 0.9$
<b>III</b>	$51.6 \pm 0.3$	$49.9 \pm 0.4$	$23.2 \pm 0.7$	$141.6 \pm 0.7$	$135.8 \pm 0.5$
LDH–Cl	$63.83 \pm 0.08$	$62.93 \pm 0.2$	$30 \pm 1$	$138.2 \pm 0.2$	$139.2 \pm 0.3$

<sup>a</sup> Calculations were performed at ambient conditions, with  $n = 9$ . A thickness of 4.05 Å was used to calculate the Young's moduli of the LDH Sheets. Comparison is made with the average value of the bending moduli obtained for LDH–Cl.<sup>27</sup> Error bars are found from the error on the gradient of the stress–strain curves.

are  $E_x = 61 \pm 1$  GPa,  $E_y = 69 \pm 2$  GPa,  $E_z = 33 \pm 2$  GPa, while those of the LDH sheets alone are  $E_x = 136 \pm 3$  GPa and  $E_y = 144 \pm 3$  GPa. These values are consistent with those of the LDH–Cl models; see Table 3.<sup>27</sup> The main difference between LDH–Cl and LDH–DNA with  $n = 2$  is that the latter is more rigid in the  $y$ -dimension, probably because the major axis of the DNA molecule in system **I** lies along the  $y$ -direction which prevents compression and expansion in this direction.

Determination of the thickness,  $h_{\text{clay}}$ , of LDH sheets is required when calculating elastic properties; this thickness has

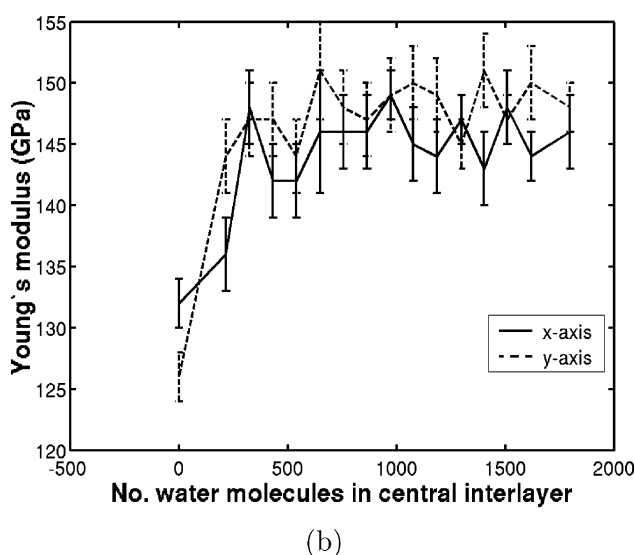
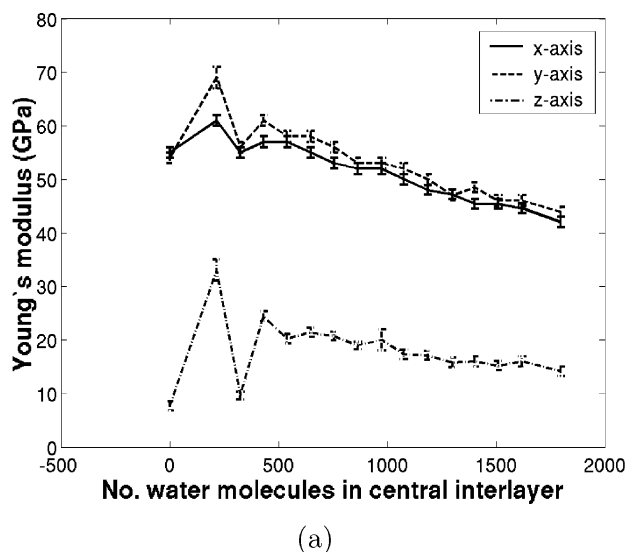


**Figure 15.** Young's moduli in  $x$ -,  $y$ - and  $z$ -directions as a function of water content for (a)  $\text{Mg}_2\text{Al}$ -LDH/DNA and (b) the  $\text{Mg}_2\text{Al}$  sheets alone in system **I**. In each direction, there is a general decline in stiffness for the whole LDH–DNA system as a function of water content. The LDH sheets alone exhibit much less variation in Young's moduli with hydration, showing that the elastic properties of the LDH sheets are not affected by water content in the  $xy$  plane. Error bars are determined from the error on the gradient of the stress–strain curves.

previously been found to be 4.05 Å.<sup>27</sup> The stress–strain analyses of the LDH–DNA systems performed here used this thickness to compute elastic properties. The stress experienced by individual atoms in the LDH sheets was used to calculate elastic properties of the LDH sheets alone. Figure 15b shows how the Young's modulus of the LDH sheets varies with hydration for system **I**. The individual LDH sheets show an increase in rigidity between 0 and 400 water molecules but very little change in rigidity after this point, the values fluctuating around 145.4 GPa in the  $x$ -direction and 148.1 GPa in the  $y$ -direction. This suggests that, when there are more than 400 water molecules in the central interlayer of system **I**, hydration does not affect the rigidity of the LDH layers. Our present study was unable to obtain an accurate value of  $E_z$  for the LDH sheets alone as the stress–strain simulations deform the entire simulation cell in the  $z$ -dimension, the applied force pulling individual LDH sheets

**Table 4.** Bending Modulus Calculated from Stress–Strain Behavior of the LDH Sheets

system	bending modulus (J)	
	$k_x$	$k_y$
<b>I</b>	$8.8 \pm 0.004 \times 10^{-19}$	$9.1 \pm 0.004 \times 10^{-19}$
<b>II</b>	$7.9 \pm 0.2 \times 10^{-19}$	$8.0 \pm 0.2 \times 10^{-19}$
<b>III</b>	$7.9 \pm 0.2 \times 10^{-19}$	$7.6 \pm 0.2 \times 10^{-19}$
LDH–Cl <sup>−</sup>	$8.40 \pm 0.03 \times 10^{-19}$	$8.17 \pm 0.03 \times 10^{-19}$

<sup>a</sup> A thickness of 4.05 Å was used to calculate values for the in-plane Young's moduli of the LDH sheets, as well as the bending modulus.<sup>27</sup> A comparison is made with the average value of the bending moduli obtained for LDH–Cl.<sup>27</sup> All systems show very similar values to the LDH–Cl properties previously reported. This indicates that the bending modulus of the LDH sheets is unaffected by the intercalation of DNA.

apart but not acting on the LDH sheets directly. Future studies would need to deform a single LDH sheet alone to obtain this value.

Table 3 compares the Young's moduli for different system sizes. A general decrease in rigidity is seen for the LDH sheets in the  $x$ - and  $y$ -dimensions for increasing system size. The average Young's moduli for the LDH sheets were found to be  $144 \pm 2$  GPa in the  $x$ -direction and  $143 \pm 1$  GPa in the  $y$ -direction. The slight difference in  $E_x$  and  $E_y$  is within the error in the gradient of the stress–strain curves. The rigidity in the  $x$ - and  $y$ -dimensions of both the LDH sheets and the system as a whole declines with system size. A possible explanation for this is that the orientation of the DNA strands rather than their length causes a change in flexibility. The difference in DNA molecules in each system also contributes to variations in Young's moduli.

$E_z$  was found in this study for both LDH–DNA and LDH–Cl in order to make a comparison between both systems. We expect  $E_z$  to be much smaller than  $E_x$  and  $E_y$ , as it is easier to cleave layers apart than fracture sheets. Although our simulation models would benefit from being extended in the  $z$ -axis, the cell dimensions used in this study are sufficient to obtain reasonably accurate values for  $E_z$ . Typical LDH–DNA systems form platelets around  $100 \text{ nm} \times 100 \text{ nm} \times 20 \text{ nm}$  in size,<sup>77</sup> so their lateral dimensions are much larger than in the perpendicular direction. With the scale of computational resources now available, it is becoming possible to perform simulations of finite clay systems including explicit edges; this is left for future study.

The Poisson ratios and bending moduli of the systems were also calculated.<sup>27</sup> In general, all systems have similar Poisson ratios,  $\nu_{yx} \approx \nu_{zx} \approx \nu_{xy} \approx \nu_{zy} = 0.29$  and  $\nu_{xz} \approx \nu_{yz} = 0.095$ . The bending moduli, shown in Table 4, were found to be similar for all three model sizes, albeit that the smallest, system **I**, exhibits an increased bending rigidity compared to the larger models. This may be explained by the ratio of intercalated DNA to LDH. In system **I**, DNA atoms comprise 7.5% of all atoms, whereas in systems **II** and **III** the percentage of DNA atoms is 2.0% and 2.7%, respectively. The bending moduli in the  $x$ - and  $y$ -dimensions of systems **II** and **III** have similar values, which are within errors in the least-squares fit. On average, all models have a bending modulus of  $8.2 \times 10^{-19}$  J in both the  $x$ - and  $y$ -dimensions. This is very similar to the bending moduli found in our previous study of LDH–Cl,<sup>27</sup> which has  $k_x$  and  $k_y$  equal to  $8.40 \pm 0.03 \times 10^{-19}$  J and  $8.17 \pm 0.03 \times 10^{-19}$  J,

respectively, suggesting that intercalation of DNA does not have a significant effect on this particular elastic constant.

#### 4. Conclusions

We have shown that strong electrostatic forces act between LDH sheets and intercalated DNA, causing the DNA molecules in all systems to be significantly restricted in movement compared to DNA in bulk water. Structural analysis of intercalated DNA molecules in all systems, averaged over 1 ns, show that the motion of phosphate groups in the DNA backbone is extremely restricted as compared to simulations of DNA in bulk water. Varying the hydration state of the smallest model demonstrates that hydration plays a crucial part in the stability of the molecule. In the anhydrous state, all Watson–Crick hydrogen bonds are disrupted. The basal spacing is also dependent on the extent of hydration of the interlayer, manifesting steps in the swelling curve which correspond to transitions between varying numbers of water layers.

Increasing the temperature and pressure of the simulations confirms that the structure of the DNA is stabilized once intercalated. All simulations show an increase in average rmsd at higher temperatures, relative to their initial structure. Contrasting behavior is seen, however, between the larger and smaller systems so far as the effect of temperature on the number of Watson–Crick base pairs is concerned. As the long strand of DNA containing 108 base pairs is subjected to higher temperatures and pressures, an increase in the LDH basal spacing is observed, together with an increase in the number of Watson–Crick hydrogen-bonded base pairs, indicative of enhanced structural stability. Since the number of Watson–Crick hydrogen bonds rapidly degrades for DNA in bulk water under similar conditions, our simulations indicate that DNA intercalated into LDHs is endowed with enhanced structural stability.

Materials properties for LDHs have been difficult to obtain experimentally due to their small size. The techniques we have used in this paper and earlier work<sup>27,28</sup> provide estimates for the in-plane Young's and bending moduli. Previously, we have shown that the LDH–Cl studied here is around 6 times less flexible than graphite, but more than twice as flexible as montmorillonite.<sup>27</sup> As a direct consequence of the flexibility of the LDH layers, the layers distort around large intercalated anions such as DNA, making the concept of basal spacing ambiguous. This is reflected in the very broad PXRD spectra reported for these systems. The distortion seen in the LDH layers may also affect the mechanism by which large molecules such as DNA intercalate during anion exchange.

Hydration plays an important role in the amount of distortion from planarity seen in the LDH sheets. When a large number of water molecules occupy the interlayer region, the LDH layers are forced apart, in turn causing less distortion in the sheets. There must be sufficient water molecules in all layers to permit corrugation of the LDH sheets; in anhydrous systems buckling is suppressed because chloride ions bind adjacent LDH layers together, preventing bending of the sheets.

The largest LDH–DNA model, containing a DNA plasmid with 480 bps, exhibits larger amplitude height fluctuations in the LDH sheets than are seen in smaller models. Compared to the same LDH system intercalated with Cl<sup>−</sup> ions alone,<sup>27</sup> the

(77) Kwak, S. Y.; Kriven, W. M.; Wallig, M. A.; Choy, J. H. *Biomaterials* **2004**, *25*, 5995–6001.

Young's moduli of these LDH–DNA systems decrease in all three dimensions, showing that the system becomes more flexible.

Our simulations provide some support for the origins-of-life theory that LDHs could have acted as a protective environment for the first nucleic acids in extreme environmental conditions such as those found around deep-ocean hydrothermal vents.<sup>21,22,26</sup> The stability of intercalated DNA is also of relevance to drug delivery and, specifically, gene therapy. Our simulations indicate that plasmids are structurally supported when intercalated under ambient conditions, explaining the high efficacy rate of LDHs in gene transport observed experimentally.<sup>1,2,67</sup>

**Acknowledgment.** This work was in part supported by the UK Engineering and Physical Sciences Research Council (EPSRC) (GR/T27488/01), which also provided access to HPCx (www.hpcx.ac.uk) and by EPSRC grant Number GR/T04465/01 (ESLEA). We are also indebted to the National Science Foundation for TeraGrid allocations under NRAC Grant MCA04N014 and MRAC Grant DMR070013N, utilizing re-

sources on the U.S. TeraGrid (www.teragrid.org), the UK's National Grid Service (www.ngs.ac.uk) and the DEISA Consortium (co-funded by the EU, FP6 project 508830) within the DEISA Extreme Computing Initiative (www.deisa.org). M.-A.T. was funded by an EPSRC PhD studentship associated with the Reality Grid Project (GR/67699/02).

**Supporting Information Available:** MPEG animations of height functions of systems (I–III) and MD trajectories for 0–2 ns of systems (I–III); the breakdown of the potential energy into its components for system I at different hydration states at 300 K, averaged over 1 ns of MD simulation; a table of all the charges of the LDH atoms and DNA phosphate groups; the first three eigenvectors from the principal component analysis and AtomEye snapshots of system II taken after 1 ns of simulation at different temperatures. This material is available free of charge via the Internet at <http://pubs.acs.org/>.

JA077679S